JOURNAL OF SOLID STATE CHEMISTRY 113, 444–447 (1994)

BRIEF COMMUNICATION

Synthesis, Structure, and Magnetism of $Ba_2VO(PO_4)_2 \cdot H_2O$, a New Barium Vanadium(IV) Phosphate Hydrate

William T. A. Harrison,*,[1] Shiao C. Lim,* J. T. Vaughey,* Allan J. Jacobson,*,[1] David P. Goshorn,† and Jack W. Johnson†

*Department of Chemistry, University of Houston, Houston, Texas 77204-5641; and †Corporate Research Laboratories, Exxon Research and Engineering Company, Annandale, New Jersey 08801

Received January 24, 1994; in revised form April 11, 1994; accepted April 12, 1994

The hydrothermal synthesis, which requires the presence of zinc nitrate and tetraethylammonium hydroxide, and the single-crystal structure of $Ba_2VO(PO_4)_2 \cdot H_2O$ are described. The $Ba_2VO(PO_4)_2 \cdot H_2O$ structure is built up from discrete, infinite $VO(PO_4)_2 \cdot H_2O$ chains, built up from VO_6 and PO_4 moieties, separated by 11-coordinate Ba^{2+} cations. Magnetic susceptibility data for $Ba_2VO(PO_4)_2 \cdot H_2O$ are consistent with V^{IV} and show magnetic ordering below ~10 K and paramagnetic behavior from ~15–300 K. Crystal data: $Ba_2VO(PO_4)_2 \cdot H_2O$, $M_r = 549.56$, monoclinic, space group $C2/m$ (No. 12), $a = 12.420(3)$ Å, $b = 5.219(2)$ Å, $c = 6.941(2)$ Å, $\beta = 104.52(2)°$, $V = 435.55$ Å^3, $Z = 2$, $R = 2.14\%$, $R_w = 2.45\%$ (879 reflections with $I > 3\sigma(I)$). © 1994 Academic Press, Inc.

INTRODUCTION

A remarkable variety of phases have been synthesized and structurally characterized in the *M*/vanadium/phosphate (*M* = uni- or divalent cation) phase space over the past few years (1, 2, 3). Known barium/vanadium/phosphates include the layered vanadium(V)-containing $Ba(VO_2)PO_4$ (4), the channel-containing vanadium(IV) material $BaV_2P_2O_{10}$ (5), and the V^{III}-containing phases $BaV_2P_4O_{14}$ (6), $Ba_2V_3H(PO_4)_2(P_2O_7)_2$ (7), and $BaV_2(HPO_4)_4 \cdot H_2O$ (8). These three vanadium(III) materials all contain different, vertex-sharing, three-dimensional VO_6/$(H)PO_4$ frameworks. The V^{IV}-containing $Ba_8(VO)_6(PO_4)_2(HPO_4)_{11} \cdot 3H_2O$ (9) contains a complex arrangement of two different types of one-dimensional chains of vertex-sharing VO_6 and $(H)PO_4$ groups, separated by barium cations.

In this paper we report the hydrothermal preparation, X-ray single crystal structure, and some properties of $Ba_2VO(PO_4)_2 \cdot H_2O$, a new barium/vanadium(IV)/phosphate phase, which contains one-dimensional $VO(PO_4)_2 \cdot H_2O$ chains, and 11-coordinate barium cations. It appears that the presence of $Zn(NO_3)_2$ and tetraethylammonium hydroxide in the reaction mixture are required for $Ba_2VO(PO_4)_2 \cdot H_2O$ to form, but no zinc is incorporated into the single-crystal product.

EXPERIMENTAL

Blue-green, block-like single crystals of $Ba_2VO(PO_4)_2 \cdot H_2O$ were prepared from a reaction mixture comprising of 0.50 g V_2O_5 (98+%, Aldrich), 0.045 g V (99.5%, Aldrich), 2.18 g $BaCO_3$ (99.9%, Aldrich), 1.5 ml H_3PO_4 (85%, Fisher), 1.60 g $Zn(NO_3)_2$ (99.9%, Aldrich), and 6 ml distilled water. The pH of the initial mixture was adjusted to 4.0 by drop-wise addition of ~3 ml tetraethylammonium hydroxide (TEAOH) solution, and the reactants were sealed in a 23-ml capacity Teflon-lined Parr hydrothermal bomb. The bomb, which was approximately 50% full, was heated to 200°C for 4 days and then slowly cooled to room temperature over a 2-day period. The bomb contents were recovered by vacuum filtration and drying in air. The yield of the title compound and other phases, including unidentified clear crystals and white powder, was approximately 50%, of which ~25% was $Ba_2VO(PO_4)_2 \cdot H_2O$.

Hydrothermal reactions which omitted the zinc nitrate, but with the same ratio of Ba : V : P precursors as the above synthesis, led to different, green needle-like crystals which were not the $Ba_2VO(PO_4)_2 \cdot H_2O$ phase. Preliminary elemental analysis indicated a Ba : V : P ratio of ~1 : 2 : 2 in this single-crystal product. Reactions which started from a 2 : 1 : 2 stoichiometric mixture of Ba, V, and P precursors (or a 2 : 1 Ba : V ratio and excess phosphate), but without the addition of $Zn(NO_3)_2$, led to further different products, including yellow crystals of the known

[1] To whom correspondence should be addressed.

0022-4596/94 $6.00

$Ba(VO_2)PO_4$ (4) and other unidentified phases. Reactions at pH 2 or below (no TEAOH added) also led to $Ba(VO_2)PO_4$ as the major product. Reactions at pH 4, in which the TEAOH was replaced by NH_4OH or NaOH, led to yellow crystals of $Ba(VO_2)PO_4$ and other phases.

At this stage, the role of the zinc nitrate and the TEAOH in the reaction are not obvious, although it appears that both must be present to obtain a partial yield of crystals of $Ba_2VO(PO_4)_2 \cdot H_2O$. Zn^{2+} may control phosphate concentration in solution, while the TEAOH that is used to adjust the pH does not form any stable intermediate compounds (TEA/V/PO_4 phases) that would compete with the $Ba_2VO(PO_4)_2 \cdot H_2O$ phase isolated here. It is obvious that the Ba/V/P/O hydrothermal-reaction phase space is highly sensitive to precise reaction conditions: We have observed similar "structure directing" effects in hydrothermal M/V/PO_4 (M = Sr, Cs, Rb) preparations caused by the addition of zinc nitrate, and the effect is being investigated further.

Magnetic susceptibility data, collected using isolated single crystals of $Ba_2VO(PO_4)_2 \cdot H_2O$, were obtained between 4.2 and 300 K (applied field 6 kG) using a Quantum Design model MPMS SQUID magnetometer. Ferromagnetic impurity contributions to the magnetic susceptibility were measured and corrected for by using magnetization isotherms obtained at 77 and 298 K.

The crystal structure of $Ba_2VO(PO_4)_2 \cdot H_2O$ was determined from single-crystal X-ray diffraction data: A blue block (dimensions ~0.3 × 0.2 × 0.1 mm) was mounted on a thin glass fiber with cyanoacrylate adhesive, and room-temperature [25(2)°C] intensity data were collected on an Enraf–Nonius CAD4 automated 4-circle diffractometer (graphite-monochromated Mo$K\alpha$ radiation, λ = 0.71073 Å), as outlined in Table 1. Intensity maxima were scanned (n = 2082; $2\theta < 60°$; $\pm h$, $\pm k$, $+l$), and the systematic absence condition in the reduced data (hkl, $h + l \neq 2n$) indicated space groups $C2$, Cm, or $C2/m$. An absorption correction (min. = 2.03, max. = 3.08), based on ψ-scans, was applied at the data reduction stage.

The crystal-structure model of $Ba_2VO(PO_4)_2 \cdot H_2O$ was successfully developed in space group $C2/m$ (No. 12), which was then assumed for the remainder of the crystallographic analysis. Initial heavy-atom positions (Ba, V, P) were located using the direct-methods program SHELXS-86 (*10*) using an approximate atomic composition to facilitate E-map calculation. The four oxygen-atom positions were located from Fourier difference maps during the refinement. The vanadium atom is disordered over two symmetry-related, adjacent positions (*vide infra*). The final cycles of full-matrix least-squares refinement were against F and included anisotropic temperature factors and a Larson-type secondary extinction correction (*11*) (refined value 6.9 (3)). Complex, neutral-atom scattering factors were obtained from the "International Tables" (*12*). At the end of the refinement, analysis of the various trends in F_o versus F_c revealed no unusual effects. The least-squares, Fourier and subsidiary calculations were performed using the Oxford CRYSTALS system (*13*), running on a DEC Micro VAX 3100 computer. Final residuals of R = 2.14% and R_w = 2.45% ($w_i = 1/\sigma_i^2$) were obtained.

TABLE 1
Crystallographic Parameters for $Ba_2VO(PO_4)_2 \cdot H_2O$

Empirical formula	$Ba_2V_1P_2O_{10}H_2$
Formula weight	549.56
Habit	Blue-green block
Crystal system	Monoclinic
a (Å)	12.420(3)
b (Å)	5.219(2)
c (Å)	6.942(2)
β (°)	104.52(2)
V (Å^3)	435.55
Space group	$C2/m$ (No. 12)
Z	2
hkl limits	$-20 \rightarrow 19$, $0 \rightarrow 8$, $0 \rightarrow 11$
T (°C)	25(1)
ρ_{calc} (g/cm^3)	4.19
μ(Mo$K\alpha$) (cm^{-1})	103.7
Min., max. $\Delta\rho$ (electron/Å^3)	−1.5, 1.1
Total data	2082
Observed data[a]	879
$R(F)$[b] (%)	2.14
$R_w(F)$[c] (%)	2.45

[a] $I > 3\sigma(I)$ after merging |, (R_{int} = 3.36%).
[b] $R = \Sigma\|\|F_o| - |F_c\|/\Sigma|F_o|$.
[c] $R_w = [\Sigma_w(|F_o| - |F_c|)^2/\Sigma w|F_o|^2]^{1/2}$, with $w_i = 1/\sigma_i^2$.

RESULTS

Crystal structure. Final atomic positional and equivalent isotropic thermal parameters for $Ba_2VO(PO_4)_2 \cdot H_2O$ are listed in Table 2, with selected bond distance/angle

TABLE 2
Atomic Positional/Thermal Parameters for $Ba_2VO(PO_4)_2 \cdot H_2O$

Atom	x	y	z	U_{eq}[a]
Ba(1)	0.17299(3)	0	0.21952(5)	0.0131
V(1)[b]	0.0078(1)	½	0.4540(2)	0.0090
P(1)	0.1350(1)	0	0.7133(2)	0.0102
O(1)	0.1220(2)	0.2388(5)	0.5757(4)	0.0146
O(2)	0.2517(3)	0	0.8506(5)	0.0151
O(3)	0.0496(3)	0	0.8350(5)	0.0192
O(4)	0.0239(3)	½	0.2354(6)	0.0203

[a] U_{eq}(Å^2) = $(U_1U_2U_3)^{1/3}$.
[b] Disordered about the (0, ½, ½) special position (50% site occupancy).

TABLE 3
Bond Distances (Å)/Angles(°) for $Ba_2VO(PO_4)_2 \cdot H_2O$

Ba(1)–O(1) × 2	2.975(3)	Ba(1)–O(1)′ × 2	2.924(3)
Ba(1)–O(2)	2.961(4)	Ba(1)–O(2)′ × 2	2.855(2)
Ba(1)–O(3)	2.724(4)	Ba(1)–O(3)′	2.694(4)
Ba(1)–O(4) × 2	3.217(2)		
V(1)–O(1) × 2	1.995(3)	V(1)–O(1)′ × 2	2.082(3)
V(1)–O(4)	1.580(4)	V(1)–O(4)′	2.287(4)
P(1)–O(1) × 2	1.554(3)	P(1)–O(2)	1.522(4)
P(1)–O(3)	1.514(4)		
O(1)–V(1)–O(1)′	160.00(9)	O(1)–V(1)–O(1)′	92.6(1)
O(1)–V(1)–O(1)′	81.8(2)	O(1)–V(1)–O(1)′	86.2(2)
O(1)–V(1)–O(4)	99.2(2)	O(1)–V(1)–O(4)	100.7(1)
O(1)–V(1)–O(4)	82.7(1)	O(1)–V(1)–O(4)	77.3(1)
O(4)–V(1)–O(4)′	177.4(1)		
O(1)–P(1)–O(1)′	106.7(2)	O(1)–P(1)–O(2)	108.7(1)
O(1)–P(1)–O(3)	111.3(1)	O(2)–P(1)–O(3)	109.9(2)
V(1)–O(1)–P(1)	139.6(2)	V(1)–O(1)–P(1)	123.0(2)

data given in Table 3. $Ba_2VO(PO_4)_2 \cdot H_2O$ is built up from barium cations and chains of vertex-sharing VO_6 and PO_4 units, and the complete crystal structure is illustrated with ORTEP (14) in Fig. 1.

The component species in $Ba_2VO(PO_4)_2 \cdot H_2O$ (1 Ba, 1 V, 1 P, 4 O) show their typical crystallochemical behavior. The barium cation (site symmetry *m*) is coordinated by 11 oxygen atoms within 3.25 Å, with an average *d*(Ba–O) of 2.938(1) Å, in irregular "4 + 4 + 3" geometry (Fig. 2). A Brese–O'Keefe bond valence sum (BVS) calculation (15) for the barium cation gives a value of 2.08, compared to the expected 2.00. One of the O(2) atoms and both the O(3) atoms also lie on the mirror plane (Table 3).

The crystallographically distinct vanadium atom (site symmetry *m*) is octahedrally coordinated and shows the short, vanadyl, "double" V(1) = O(4) bond [*d* = 1.580(4) Å] characteristic of V^{IV} or V^{V} (16), *trans* to a long V(1)–O(4) bond, this latter oxygen atom being part of a water molecule. V(1)'s four remaining oxygen-atom vertices, all of which are O(1)'s, each make a bridging link to (different) adjacent phosphorus atoms. The Brese–O'Keefe BVS value for the V atom is 4.02, using parameters appropriate for V^{IV} (15), indicative of pure vanadium(IV) character for this atom. The vanadium atom is disordered and occupies a site randomly displaced from the $(0, \frac{1}{2}, \frac{1}{2})$ special position, with an apparent V ··· V separation of ~0.7 Å. Therefore, the O(4) site (Table 2) represents the average position of the oxygen atoms involved in the short V = O bond, and the long V–OH_2 bond. No protons could be located from the X-ray data, which are dominated by the scattering of the heavy atoms, nor could they be geometrically placed unambiguously, by consideration of possible H-bonding links (several O(4) ··· O contacts in the range 2.74–3.17 Å are present).

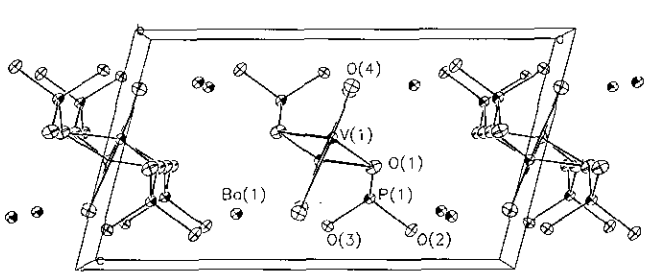

FIG. 1. Unit-cell packing of $Ba_2VO(PO_4)_2 \cdot H_2O$, viewed down [010], showing the infinite $VO(PO_4)_2 \cdot H_2O$ chains, separated by Ba^{2+} cations. Fifty percent thermal ellipses, with selected atoms labeled.

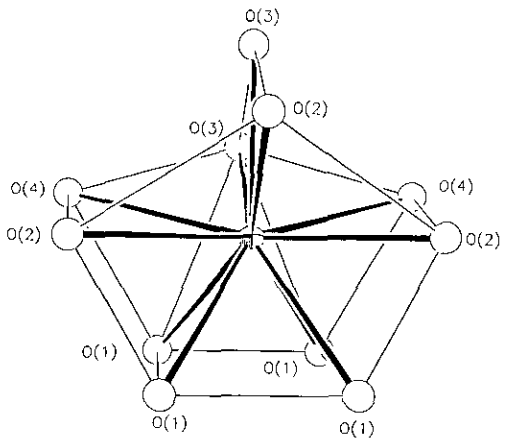

FIG. 2. Eleven-coordinate Ba(1) coordination polyhedron in $Ba_2VO(PO_4)_2 \cdot H_2O$, with nonbonding O ··· O contacts <3.8 Å indicated by thin lines. Oxygen atoms are represented by spheres of arbitrary radius.

The phosphorus atom in $Ba_2VO(PO_4)_2 \cdot H_2O$ shows its standard tetrahedral coordination, with two bridging P(1)–O(1) bonds to nearby vanadium atoms, and two terminal P–O bonds, which otherwise only bond to barium cations. The short (d < 1.53 Å) P(1)–O(2) and P(1)–O(3) bond lengths (Table 3) indicate that these latter oxygen atoms are not protonated. A typical d_{av}(P–O) of 1.586(2) Å and a BVS of 4.81 result for this P atom.

The polyhedral connectivity in $Ba_2VO(PO_4)_2 \cdot H_2O$ leads to infinite chains of stoichiometry $[VO(PO_4)_2 \cdot H_2O]^{2-}$, separated by the Ba^{2+} cations. Each $VO_5 \cdot H_2O$ center is bridged to its neighbors by pairs of PO_4 groups; thus the vanadium–vanadium linkage is via V–O–P–O′–V′ bonds. These chains (Fig. 3) propagate in the **b** direction and are completely separated from each other (Fig. 1), except via O–Ba–O connections. The overall symmetry of each chain is 2/*m*.

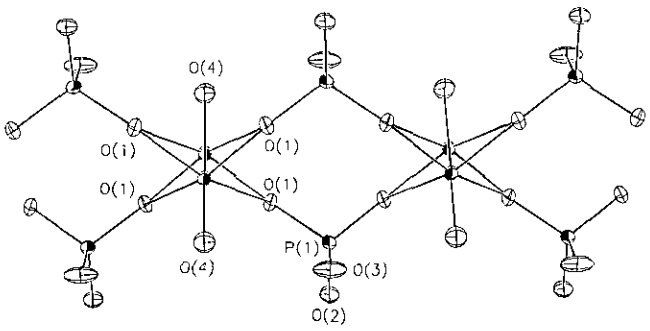

FIG. 3. Detail of the $VO(PO_4)_2 \cdot H_2O$ chain structure in $Ba_2VO(PO_4)_2 \cdot H_2O$, showing "4-rings" of VO_6 and PO_4 polyhedra and disordered vanadium atoms (50% thermal ellipsoids).

Magnetic measurements. Susceptibility data for $Ba_2VO(PO_4)_2 \cdot H_2O$ (Fig. 4) showed the onset of magnetic ordering at ~10 K and perfect Curie–Weiss-type paramagnetic behavior over the range ~15–300 K. The paramagnetic data were modeled by using a Curie–Weiss-type law: $\chi = \chi_0 + C/(T - \theta)$, where χ is the measured magnetic susceptibility, C is the Curie constant, T the temperature (K), and θ the Weiss constant. The model yielded best-fit values of $\chi_0 = -5.269 \times 10^{-8}$ emu/g, $C = 8.387 \times 10^{-4}$ emu-K/g, and $\theta = -8.5$ K, corresponding to a μ_{eff} of 1.92 Bohr magnetons, slightly higher than the ideal value for vanadium(IV) of 1.73 BM. The sample used for the magnetic measurements was physically separated from the mixed-phase reaction product. The small discrepancy between the expected and observed moment is most likely due to the presence of a trace amount of a paramagnetic (V^{3+}) impurity.

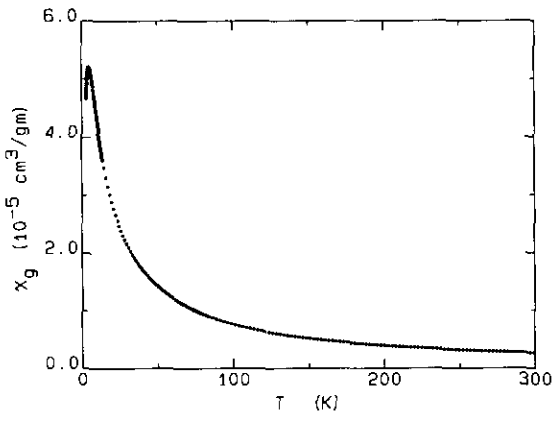

FIG. 4. Magnetic susceptibility data for $Ba_2VO(PO_4)_2 \cdot H_2O$, plotted as χ versus temperature.

CONCLUSION

$Ba_2VO(PO_4)_2 \cdot H_2O$ further expands the variety of phases in the Ba/V/PO_4 phase space (*vide supra*) which contain octahedral vanadium centers linked via phosphate tetrahedra, with charge balance provided by barium cations. As noted above, some of these phases are three-dimensional and others are layered. $Ba_2VO(PO_4)_2 \cdot H_2O$, like the related $Ba_8(VO)_6(PO_4)_2(HPO_4)_{11} \cdot 3H_2O$, has an interesting one-dimensional structure, in which interchain connectivity is maintained only via the barium cations. Pure V^{IV} character is well defined for the vanadium centers in $Ba_2VO(PO_4)_2 \cdot H_2O$ (bond-valence-sum calculations, susceptibility data), and magnetic ordering is observed at low temperatures, presumably via V–O–P–O′–V′ superexchange. The shortest V–V separation is 5.219(2) Å, defined by the b unit-cell parameter. Other barium/vanadium/phosphate phases are now being investigated and will be described later.

ACKNOWLEDGMENTS

We thank Ivan Bernal (University of Houston) for access to X-ray data collection facilities. This work is partially funded by the National Science Foundation (DMR-9214804) and the Welch Foundation.

REFERENCES

1. K. H. Lii, N. S. Wen, C. C. Su, and B. R. Chen, *Inorg. Chem.* **31,** 439 (1992), and included references.
2. V. Soghomonian, Q. Chen, R. C. Haushalter, J. Zubieta, and C. J. O'Connor, *Science (Washington, DC)* **259,** 1596 (1993).
3. R. C. Haushalter, Z. Wang, M. E. Thompson, and J. Zubieta, *Inorg. Chem.* **32,** 3700 (1993), and included references.
4. H. Y. Yang, S. L. Wang, and K. H. Lii, *Acta Crystallogr. Sect. C* **48,** 975 (1992).
5. A. Grandin, J. Chardon, M. M. Borel, A. LeClair, and B. Raveau, *J. Solid State Chem.* **99,** 297 (1992).
6. L. Benhamada, A. Grandin, M. M. Morel, A. LeClair, and B. Raveau, *Acta Crystallogr. Sect. C* **47,** 2438 (1991).
7. E. Dvoncova, K.-H. Lii, C.-H. Li, and T.-M. Chen, *J. Solid State Chem.* **106,** 485 (1993).
8. Z. Wang, R. C. Haushalter, M. E. Thompson, and J. Zubieta, *Mater. Chem. Phys.* **35,** 205 (1993).
9. W. T. A. Harrison, J. T. Vaughey, A. J. Jacobson, D. P. Goshorn, and J. W. Johnson (1994) *J. Solid State Chem.*, in press.
10. G. M. Sheldrick, "SHELXS-86 User Guide," Crystallography Department, University of Göttingen, Germany, 1986.
11. A. C. Larson, *Acta Crystallogr.* **23,** 664 (1967).
12. "International Tables for X-Ray Crystallography," Vol. IV, Kynoch Press, Birmingham, 1974.
13. D. J. Watkin, J. R. Carruthers, and P. W. Betteridge, "CRYSTALS User Guide, Version 9.0," Chemical Crystallography Laboratory, Oxford University, UK, 1993.
14. C. K. Johnson, Report ORNL-5138, Oak Ridge National Laboratory, Oak Ridge, TN, 1976, with local modifications.
15. N. Brese and M. O'Keefe, *Acta Crystallogr. Sec B* **47,** 192 (1991).
16. A. J. Jacobson, J. W. Johnson, J. F. Brody, J. C. Scanlon, and J. T. Lewandowski, *Inorg. Chem.* **24,** 1782 (1985).